



1                   **Diagnosis toward predicting mean annual runoff in ungauged basins**

2                   Yuan Gao, Lili Yao, Ni-Bin Chang and Dingbao Wang\*

3                   Department of Civil, Environmental, and Construction Engineering, University of Central

4                   Florida, Orlando, FL 32816, United States

5                   \*Correspondence to D. Wang, [dingbao.wang@ucf.edu](mailto:dingbao.wang@ucf.edu)

6                   **Abstract**

7                   Prediction of mean annual runoff is of great interest but still poses a challenge in ungauged basins.  
8                   The present work diagnoses the prediction in mean annual runoff affected by the uncertainty in  
9                   estimated distribution of soil water storage capacity. Based on a distribution function, a water  
10                  balance model for estimating mean annual runoff is developed, in which the effects of climate  
11                  variability and the distribution of soil water storage capacity are explicitly represented. As such,  
12                  the two parameters in the model have explicit physical meanings, and relationships between the  
13                  parameters and controlling factors on mean annual runoff are established. The estimated  
14                  parameters from the existing data of watershed characteristics are applied to 35 watersheds. The  
15                  results showed that the model could capture 88.2% of the actual runoff on average, indicating that  
16                  the proposed new water balance model is promising for estimating mean annual runoff in  
17                  ungauged watersheds. The underestimation of runoff is mainly caused by the underestimation of  
18                  the spatial heterogeneity of soil storage capacity due to neglecting the effect of land surface and  
19                  bedrock topography. A higher spatial variability of soil storage capacity estimated through the  
20                  Height Above the Nearest Drainage (HAND) indicated that topography plays a crucial role in  
21                  determining the actual soil water storage capacity. The performance of mean annual runoff  
22                  prediction in ungauged basins can be improved by employing better estimation of soil water  
23                  storage capacity including the effects of soil, topography and bedrock. The purpose of this study



24 is to diagnose the data requirement for predicting mean annual runoff in ungauged basins based  
25 on a newly developed process-based model.

26 **Keywords:** mean annual runoff; ungauged; storage capacity; curve number; soil; topography;  
27 bedrock

28

## 29 **1. Introduction**

30 Hydrologists have a long-standing interest in mean annual water balance modeling and  
31 prediction. The factors controlling mean annual runoff have been studied in the literature. Mean  
32 climate has been identified as the first order control on mean annual runoff and evaporation and it  
33 has been quantified by climate aridity index, which is defined as the ratio between the mean annual  
34 potential evapotranspiration and precipitation (Turc, 1954; Pike, 1964). Other controlling factors  
35 include the temporal variability of climate (Farmer et al., 2003; Troch et al., Fu and Wang, 2019),  
36 vegetation (Zhang et al., 2001; Donohue et al., 2007; Gentine et al., 2012; Li et al., 2013), soil  
37 (Atkinson et al., 2002; Yokoo et al., 2008; Li et al., 2014), and topography (Woods, 2003;  
38 Abatzoglou and Ficklin, 2017). Mean annual runoff or evaporation has been modeled as a function  
39 of climate aridity index and the equation is usually called as Budyko equation (Budyko, 1958).  
40 The effects of other factors are represented by including a parameter to Budyko equations (Fu,  
41 1981; Yang et al., 2008; Wang and Tang, 2014). Among these factors, climate including its mean  
42 and temporal variability, and soil water storage capacity including its mean and spatial variability  
43 are dominant catchment characteristics controlling mean annual runoff, especially for saturation  
44 excess runoff generation-dominated catchments (Milly, 1994).

45 Intra- and inter-annual climate variability introduces non-steady state conditions to finer  
46 timescale water balances and the non-steady state effect could propagate to the mean annual runoff.



47 The effects of seasonal variations of precipitation and potential evaporation on long-term runoff  
48 have been studied in several studies. Milly (1994) showed that seasonality tends to increase mean  
49 annual runoff through a stochastic soil moisture model. The seasonality effects have been  
50 demonstrated through a top-down model by Hickel and Zhang (2006) and a classification study by  
51 Berghuijs et al. (2014). Mean annual water balance also receives impacts from climate variability  
52 at the inter-annual and daily timescales. Li (2014) showed that the inter-annual variability of  
53 precipitation and potential evaporation could increase the mean annual runoff up to 10% based on  
54 a stochastic soil moisture model. Shao et al. (2012) found that daily precipitation with a larger  
55 variation potentially increases mean annual runoff especially in the catchments where infiltration  
56 excess runoff is prevalent. Yao et al. (2020) quantified the relative contribution of daily, monthly  
57 and inter-annual climate variabilities to mean annual runoff and showed that the contribution  
58 decreases, by average, from monthly to inter-annual scale, and then daily scale.

59 Soil water storage capacity exerts a powerful control on mean annual runoff. A smaller  
60 soil water storage capacity creates favorable conditions for runoff generation because the  
61 precipitation in excess of the available storage capacity would be lost as runoff directly, while  
62 catchments with a larger soil water storage capacity could hold more precipitation for evaporation  
63 (Sankarasubramanian and Vogel, 2002; Porporato et al., 2004; Chen et al., 2013). Soil water  
64 storage capacity is closely related to vegetation since the root structure of vegetation could affect  
65 soil water holding capacity significantly. Research has been conducted to reveal the role of soil  
66 water storage capacity through the linkage of vegetation and model parameter (Yang et al., 2008;  
67 Chen and Wang, 2015). Gerrits (2009) developed equations for transpiration and interception by  
68 considering the root zone and interception storage capacity as two of the most important catchment  
69 characteristics affecting evapotranspiration. In addition to the magnitude of the average soil water



70 storage capacity, the spatial variability of storage capacity within a catchment also influences  
71 precipitation partitioning at the event scale, and further influences the cumulative runoff at the  
72 mean annual scale (Moore, 1985; Jothityangkoon et al., 2001; Gao et al., 2016). It has also been  
73 suggested that the spatial variability of soil water storage capacity could suppress the actual  
74 evaporation and therefore promote the runoff generation indirectly (Yao et al., 2020).

75 Therefore, climate variability and soil water storage capacity need to be explicitly  
76 incorporated into the model for predicting mean annual runoff. The effect of climate variability  
77 could be taken into account by driving the model with daily precipitation and potential evaporation  
78 which are usually available. The spatial distribution of soil water storage capacity could be  
79 modelled by a distribution function, and it is usually modelled by the generalized Pareto  
80 distribution (Moore, 1985; Zhao, 1992). The distribution function includes two parameters, i.e.,  
81 the shape parameter and the maximum storage capacity over the watershed. In ungauged basins,  
82 soil water storage capacity and its spatial variability need to be estimated directly from available  
83 data. Gao et al. (2014) adopted the mass curve technique, which has been used for designing the  
84 storage capacity of reservoir, to estimate the average water storage capacity of the root zone using  
85 precipitation and potential evaporation data. The shape parameter of the distribution function has  
86 been estimated from soil data (Huang et al., 2003). However, the estimated parameters from these  
87 methods bring much uncertainty in runoff estimation, and the two parameters of the generalized  
88 Pareto distribution are usually estimated by model calibration using observed streamflow data  
89 (Wood et al., 1992; Alipour and Kibler, 2018, 2019).

90 The objective of this paper is toward developing nonparametric mean annual water balance  
91 model for predicting mean annual runoff in ungauged basins, which remains a challenge for  
92 hydrologists (Blöschl et al., 2013). The mean annual water balance model is forced by daily



93 precipitation and potential evaporation; therefore, the climate variability at different timescales is  
94 represented explicitly in the climate input. The runoff generation is quantified by a distribution  
95 function for describing the spatial distribution of soil water storage capacity (Wang, 2018). The  
96 mean and the shape parameter of the distribution function need to be estimated from the available  
97 data in ungauged basins. Therefore, the model serves as a diagnosis tool for evaluating the data  
98 requirement for estimating soil water storage capacity. The mean of the distribution is estimated  
99 from curve number and climate since the distribution function leads to the SCS curve number  
100 method. The estimation of the shape parameter is diagnosed in terms of the data requirement  
101 including soil, land surface topography, and bedrock topography. Section 2 introduces the new  
102 mean annual water balance model and the study watersheds. Results and discussion are presented  
103 in Section 3, followed by Section 4 for conclusions.

## 104 **2. Methodology**

### 105 **2.1 Mean annual runoff model**

106 As discussed in the introduction, the mean annual runoff model takes daily precipitation  
107 and potential evaporation as inputs, and calculates daily soil wetting (infiltration) and evaporation  
108 by tracking the soil water storage. Mean annual runoff is estimated by aggregating the daily values.  
109 The daily soil wetting is calculated using the concept of saturation excess runoff generation by  
110 modeling the spatial variability of soil moisture and storage capacity. To facilitate the parameter  
111 estimation of storage capacity distribution in ungauged basins, the following distribution function  
112 is used for modeling the spatial distribution of storage capacity (Wang, 2018):

$$113 \quad F(C) = 1 - \frac{1}{a} + \frac{C + (1-a)S_b}{a\sqrt{(C+S_b)^2 - 2aS_bC}} \quad (1)$$



114 where  $F(C)$  is the cumulative distribution function (CDF), representing the fraction of the  
 115 watershed area for which the storage capacity is equal to or less than  $C$ ;  $a$  is the shape parameter  
 116 of the distribution and varies between 0 and 2; and  $S_b$  is the average soil water storage capacity  
 117 over the watershed (i.e., the mean of the distribution). As shown in Wang (2018), this distribution  
 118 function leads to the SCS curve number (SCS-CN) method when the initial storage is set to zero.  
 119 Therefore, there is a linkage between  $S_b$  and the “potential maximum retention after runoff begins”  
 120 in the SCS-CN method, denoted as  $S_{CN}$ .

121 Daily soil wetting and runoff generation is computed as a function of daily precipitation  
 122 ( $P$ ), initial storage ( $S_0$ ),  $a$ , and  $S_b$ . As shown in Wang (2018), the average soil wetting ( $W$ ) is  
 123 computed by:

$$124 \quad W = \frac{P + S_b \sqrt{(m+1)^2 - 2am} - \sqrt{[P + (m+1)S_b]^2 - 2amS_b^2 - 2aS_bP}}{a} \quad (2)$$

125 where  $m = \frac{S_0(2S_b - aS_0)}{2S_b(S_b - S_0)}$ . Setting  $S_0 = 0$  and dividing  $P$  on both sides of equation (2), a Budyko-  
 126 type equation, representing  $\frac{W}{P}$  as a function of  $\frac{S_b}{P}$ , is obtained (Wang and Tang, 2014), which has  
 127 been used to model long-term soil wetting (Tang and Wang, 2017). Therefore, equation (2) can  
 128 be interpreted as a non-steady state Budyko equation which accounts for the effect of water storage.  
 129 Daily evaporation is computed as (Yao et al., 2020):

$$130 \quad E = \frac{W + S_0}{S_b} \frac{E_p + S_b - \sqrt{(E_p + S_b)^2 - 2aS_bE_p}}{a} \quad (3)$$

131 The first component on the right-hand side of equation (3),  $\frac{W + S_0}{S_b}$ , is the percentage of storage, and  
 132 the second component is the evaporation for the condition when the entire watershed is saturated,  
 133 i.e., the spatial distribution of soil water storage is same as that of storage capacity (Yao et al.,  
 134 2020). Dividing  $W + S_0$  on both-hand sides, equation (3) represents  $\frac{E}{W + S_0}$  as a function of  $\frac{E_p}{S_b}$ , and



135 the function is same as the Budyko-type equation derived by Wang and Tang (2014). Mean annual  
136 evaporation ( $\bar{E}$ ) is computed by aggregating the daily evaporation, and mean annual runoff ( $\bar{Q}$ ) is  
137 computed as the difference of mean annual precipitation and evaporation.

138 This mean annual water balance model applies two non-steady Budyko-type equations at  
139 the daily scale, one for daily soil wetting and the other for daily evaporation. Runoff routing is  
140 not necessary since the model is for long-term water balance. As a result, the mean annual water  
141 balance model includes two parameters, i.e., the shape parameter ( $a$ ) and the average soil water  
142 storage capacity ( $S_b$ ). For studies where a one-parameter Budyko equation is applied to long-term  
143 scale directly, the effects of climate variability (seasonality, inter-annual variability, and daily  
144 storminess) on mean annual water balance are attributed to the single parameter of Budyko  
145 equation (e.g., Fu, 1981; Zhang et al., 2001). This creates the challenge to estimate the single  
146 parameter in ungauged basins; whereas, the mean annual water balance model used in this paper  
147 takes daily precipitation and potential evaporation as inputs, and the effects of climate variability  
148 are taken into account explicitly. To achieve the goal of predicting mean annual runoff in  
149 ungauged basins,  $a$  and  $S_b$  need to be estimated in ungauged basins.

## 150 **2.2 Parameter estimation**

### 151 **2.2.1 Average soil water storage capacity**

152 Under a given soil moisture condition, soil water storage capacity is the sum of actual water  
153 storage and the remaining (or effective) storage capacity. The effective storage capacity  
154 corresponding to the normal antecedent moisture condition defined in the SCS-CN method,  $S_{CN}$   
155 (mm), is computed as a function of CN (SCS, 1972; Bartlett et al., 2016):

$$156 \quad S_{CN} = 25.4(1000/CN - 10) \quad (4)$$



157 where CN is computed based on land use and land cover (LULC) and hydrologic soil group (HSG)  
158 for each catchment. The LULC data can be obtained from the National Land Cover Database  
159 (Homer et al., 2015), and the HSG data can be extracted from the Gridded Soil Survey Geographic  
160 (gSSURGO) database with a spatial resolution of 10 m (USDA, 2014). In HSG, soils are assigned  
161 to one of the four groups (A, B, C, and D) and three dual classes (A/D, B/D, and C/D) according  
162 to the rate of infiltration when the soils are not protected by vegetation and receive precipitation  
163 from long-duration storms. For the cells characterized by dual classes, the CN value is calculated  
164 as the average of the two CN values corresponding to the two soil groups.

165 The average soil water storage capacity ( $S_b$ ) is the sum of the actual storage under the  
166 normal condition ( $\bar{S}$ ) and its corresponding effective storage capacity:

$$167 \quad S_b = \bar{S} + S_{CN} \quad (5)$$

168 Since the “normal antecedent moisture” can be interpreted as the steady-state soil moisture  
169 condition,  $\bar{S}$  is the long-term average storage over the watershed. The values of  $\bar{S}$  for 59 MOPEX  
170 (MOdel Parameter Estimation Experiment) watersheds are estimated based on the long-term water  
171 balance model in Yao et al. (2020); and these watersheds do not include any watersheds studied in  
172 this paper. The long-term water balance model used in their study has a same model structure but  
173 the two parameter, i.e., the mean value of the soil water storage capacity and its shape parameter  
174 in the distribution function, were obtained by model calibration. The ratio between  $\bar{S}$  and  $S_b$  is  
175 defined as the long-term storage ratio ( $\frac{\bar{S}}{S_b}$ ). It is found that the values of  $\frac{\bar{S}}{S_b}$  for all the watersheds  
176 were larger than 0.5. As shown in Figure 1,  $\frac{\bar{S}}{S_b}$  has a linear relationship with the climate aridity  
177 index:

$$178 \quad \frac{\bar{S}}{S_b} = -0.46\Phi + 1.2 \quad (6)$$





179 where  $\Phi$  is the climate aridity index. Substituting equations (5) and (6) into equation (4), one can  
180 estimate the average soil water storage capacity as a function of curve number and climate aridity  
181 index:

$$182 \quad S_b = \frac{SCN}{0.46\Phi - 0.2} \quad (7)$$

### 183 2.2.2 Shape parameter

184 The spatial variability of storage capacity is determined by the spatial distribution of point-  
185 scale pore space across the watershed. The volume of soil pores at point scale can be determined  
186 by soil thickness and porosity in different soil layers. The porosity ( $\theta_s$ ) for each layer is calculated  
187 from the soil bulk density:

$$188 \quad \theta_s(j) = 1 - \frac{\rho_b(j)}{\rho} \quad (8)$$

189 where  $j$  denotes the  $j^{\text{th}}$  soil layer;  $\rho_b(j)$  is the bulk density of the  $j^{\text{th}}$  soil layer;  $\rho$  is the particle  
190 density (2.65 g/cm<sup>3</sup>). After obtaining the porosity, the point-scale storage capacity can be  
191 calculated as the following equation (Huang et al., 2003):

$$192 \quad C = \sum_1^n z_j \cdot \theta_s(j) \quad (9)$$

193 where  $C$  is the point-scale soil storage capacity;  $n$  is the number of soil layers;  $z_j$  and  $\theta_s(j)$  are the  
194 thickness and porosity of the  $j^{\text{th}}$  soil layer, respectively. In the gSSURGO database, the soil  
195 thickness and bulk density for each layer are available for shallow soil from the land surface to ~  
196 2 m soil depth.

197 The total soil thickness at each point is the elevation difference from the land surface to the  
198 fresh bedrock. However, the bedrock topography is difficult to obtain especially at the catchment  
199 scale. Alternatively, it is assumed that the spatial distribution of the actual soil water storage  
200 capacity is same as the spatial distribution of water storage capacity computed from the gSSURGO  
201 database. In order to compare the shape parameter evaluated from the soil data with its



202 counterparts evaluated from other methods, the point-scale storage capacity is normalized with the  
203 average storage capacity over the watershed, and Equation (1) is rewritten as:

$$204 \quad F(x) = 1 - \frac{1}{a} + \frac{x+(1-a)}{a\sqrt{(x+1)^2-2ax}} \quad (10)$$

205 where  $x$  is the normalized storage capacity  $\left(\frac{C}{S_b}\right)$  at point scale;  $a$  is the shape parameter describing  
206 the spatial variability of soil water storage capacity. The shape parameter  $a$  is then estimated  
207 through fitting the point-scale storage capacity data obtained from Equation (9) by minimizing the  
208 root mean square error (RMSE).

### 209 **2.3. Study watersheds**

210 The estimations of mean annual runoff in 35 watersheds are diagnosed in this paper. The  
211 drainage area of the watersheds varies from 2044 to 9889 km<sup>2</sup>. Table 1 shows the USGS gauge  
212 number and climate aridity index of these watersheds. The human interferences are minimum  
213 (Wang and Hejazi, 2011), and saturation excess is the dominated runoff generation in these  
214 watersheds. Daily precipitation and streamflow data during 1948 – 2003 are extracted from the  
215 MOPEX dataset (Duan et al., 2006), and the daily potential evaporation during this period is  
216 calculated based on the Hargreaves method (Hargreaves and Samani, 1985) by using the daily  
217 maximum, minimum, and mean temperature. The average soil water storage capacity and the  
218 shape parameter for these watersheds are estimated from the available data of climate, LULC, soil,  
219 and topography, and the predictions of mean annual runoff are diagnosed.

## 220 **3. Results and discussion**

### 221 **3.1. Estimated average soil water storage capacity**

222 The potential maximum retention ( $S_{CN}$ ) is calculated based on the average CN in each  
223 watershed (Table 1). The average CN is computed based on LULC and hydrologic soil group.



224 For examples, Figure 2a shows the LULC map for the Fox River watershed in Wisconsin and  
225 Figure 2d shows the LULC map for the Spoon River watershed in Illinois. The dominant land  
226 uses are agriculture (49%) and forest (33%) in the Fox River watershed, and agriculture (77%) and  
227 forest (15%) in the Spoon River watershed. The hydrologic soil groups are shown in Figure 2b  
228 (Fox River watershed) and Figure 2e (Spoon River watershed). Given the same LULC, the  
229 hydrologic soil group D is more favorable for runoff generation compared with group A. The  
230 dominant hydrologic soil groups are group A (31%) and group B (19%) in the Fox River watershed,  
231 and group C/D (49%) and group B/D (20%) in the Spoon River watershed. The calculated CN for  
232 each grid cell is shown in Figure 3c (Fox River watershed) and Figure 3f (Spoon River watershed).  
233 The average CN is 61.0 for the Fox River watershed and 78.1 for the Spoon River watershed.  
234 Since the Spoon River watershed has a higher percentage of agricultural land and lower soil  
235 permeability, its average CN is higher than that for the Fox River watershed. Correspondingly,  
236 the calculated  $S_{CN}$  in the Fox River watershed (162 mm) is higher than that in Spoon River  
237 watershed (71 mm). The values of  $S_{CN}$  over the study watersheds vary from 56 mm (Auglaize  
238 River watershed) to 182 mm (Chattahoochee River watershed) as shown in Table 1.

239 The average soil water storage capacity is estimated based on the computed  $S_{CN}$  and  
240 climate aridity index shown in Equation (7). For examples, the climate aridity index in the Fox  
241 River watershed is 1.12 which is the same as that in the Spoon River watershed. The estimated  $S_b$   
242 is 721 mm in the Fox River watershed and 314 mm for the Spoon River watershed. As shown in  
243 Table 1, the estimated  $S_b$  varies from 177 mm (Chikaskia River watershed) to 1870 mm  
244 (Chattahoochee River watershed) over the study watersheds. Figure 3a shows the spatial  
245 distribution of the estimated  $S_b$ . Watersheds with higher  $S_b$  are mostly distributed in the eastern  
246 US, where the aridity index is relatively lower than that in the other watersheds.



247 **3.2. Estimated shape parameter**

248 The shape parameter ( $a$ ) for the distribution of soil water storage capacity is estimated  
249 based on the soil data in the gSSURGO database. For examples, the black circles in Figure 4 show  
250 the normalized storage capacity for the Fox River watershed (Figure 4a) and the Spoon River  
251 watershed (Figure 4b) based on the soil data in the gSSURGO database. As shown in Figure 4,  
252 the normalize CDF for both watersheds shows an S-shape. The estimated shape parameter is 1.996  
253 for the Fox River watershed (RMSE = 0.58) and 1.990 for the Spoon River watershed (RMSE =  
254 1.27) by fitting to the soil data. Higher value of shape parameter indicates less spatial variability;  
255 therefore, the spatial variability in the Spoon River watershed is higher than that in the Fox River  
256 watershed. The mean value of RMSE for the 35 study watersheds is 0.06. Figure 3b shows the  
257 estimated shape parameters for the study watersheds, which vary from 1.830 to 1.998.

258 **3.3. Diagnosing mean annual runoff prediction**

259 The estimated values of  $S_b$  and  $a$  based on climate, LULC, and soil data are applied to the  
260 mean annual water balance model. The comparison of simulated and observed mean annual runoff  
261 for the study watersheds is shown in Figure 5a. The RMSE for estimated mean annual runoff is  
262 80 mm/yr. The water balance model captures 88.2% of the mean annual runoff; therefore, the  
263 methods for estimating  $S_b$  and  $a$  based on the available data are promising for predicting annual  
264 runoff in ungauged basins.

265 The water balance model with the estimated values of  $S_b$  and  $a$  underestimates the mean  
266 annual runoff in some watersheds, and the relative underestimation error is 11.8% on average  
267 among all the study watersheds. The underestimation of mean annual runoff could be due to the  
268 biased estimation of the shape parameter. As described in Section 3, the spatial variability of soil  
269 storage capacity is assumed to be equal with the spatial variability of the pore space in the shallow



270 soil. The pore space at the point scale is calculated through the porosity and soil thickness. The  
271 thickness of the shallow soil in the gSSURGO database is quite uniformly distributed across the  
272 watershed, i.e., around 2 m; whereas, the actual soil thickness including the weathered bedrock is  
273 the elevation difference between the land surface and fresh bedrock, and can be highly  
274 heterogeneous due to the variable land surface and bedrock topography over the catchment.

275 To diagnose the effect of land surface and bedrock topography on mean annual water  
276 balance, the shape parameter is calibrated using the observed streamflow. The streamflow data  
277 during 1948-2003 are divided into three periods: 1) the warm-up period (1948-1953); 2) the  
278 calibration period (1954-1973); and 3) the validation period (1974-2003). During the calibration,  
279 the estimated  $S_b$  based on CN is used, and  $a$  is the only free parameter to be calibrated. The  
280 calibration is conducted by minimizing the absolute error of the observed and simulated mean  
281 annual runoff through a global optimization method, i.e., Shuffled Complex Evolution Method  
282 (Duan et al., 1992). As shown in Figure 5b, most of the calibrated  $a$  are smaller than the estimated  
283  $a$  based on soil data only. The performance of predicted mean annual runoff (during the validation  
284 period) is improved with the calibrated shape parameter (Figure 5c). The average of absolute error  
285 for the mean annual runoff is 7.1%.

286 The overestimation of shape parameter based on the soil porosity data underestimates the  
287 spatial variability of soil water storage capacity compared with the calibrated one as shown in  
288 Figure 4a for the Fox River watershed and Figure 4b for the Spoon River watershed. The slope at  
289 the normalized storage capacity around 1 for the estimated shape parameter is higher than that for  
290 the calibrated one. Therefore, the calibrated shape parameter indicates a larger spatial variability.  
291 The underestimation of the spatial heterogeneity of soil water storage capacity could be resulted



292 from neglecting the effect of land surface and bedrock topography which cannot be referred from  
293 the soil database (gSSURGO) where the point-scale soil thickness is around 2 m.

294 To explore the impact of land surface topography on the spatial distribution of soil water  
295 storage capacity, the soil data (i.e., porosity) is combined with the Height Above the Nearest  
296 Drainage (HAND) method proposed by Gao et al. (2019). HAND is the vertical elevation  
297 difference from a point to its nearest drainage point. The distribution of HAND was used for  
298 estimating the shape parameter of the spatial distribution of storage capacity. Therefore, the  
299 HAND method uses land surface topography data only for estimating the shape parameter. In our  
300 analysis, the porosity of the soil beyond the bottom layer in the soil database is assigned with the  
301 same value as the bottom layer. For example, if the HAND for a grid cell is 10.0 m and the porosity  
302 and depth of the bottom soil layer in the gSSURGO database is 0.2 and 2.0 m, respectively, the  
303 porosity for the soil from 2.0 m to 10.0 m depth is assigned with 0.2. Finally, the total volume of  
304 pores is calculated for each grid cell based on the soil porosity obtained from the gSSURGO  
305 database and the HAND value based on land surface topography.

306 Figure 6 shows the porosity-HAND based CDF of normalized soil water storage capacity  
307 for the Maquoketa River in Iowa (gauge #05418500). The stream initiation threshold used for  
308 calculating HAND is 40 km<sup>2</sup> which is 1% of the maximum flow accumulation (Maidment, 2002).  
309 The threshold affects the value of HAND but this is beyond the scope of this paper. The best fit  
310 value of  $a$  for the porosity-HAND based CDF is 1.779, which overestimates the spatial variability  
311 of storage capacity compared with the calibrated shape parameter ( $a=1.905$ ). This is due to the  
312 assumption of the HAND method that the bedrock between a specific point and its nearest drainage  
313 point is horizontal and intercepts with the channel bed. However, the bedrock topography may  
314 have various slopes in a watershed (Troch et al., 2002). Therefore, the true value of  $a$  (indicated



315 by the calibrated one) potentially falls between the  $a$  obtained from soil data and the  $a$  based on  
316 soil and HAND. The bedrock topography from observation or models is needed to accurately  
317 estimate the shape parameter.

#### 318 **4. Conclusion**

319 A mean annual water balance model based on the concept of saturation excess runoff  
320 generation is used for diagnosing the potential for nonparametric modeling of mean annual runoff  
321 in ungauged basins. The model takes the effect of climate variability into account explicitly since  
322 it is driven by daily precipitation and potential evapotranspiration at the daily time step. The  
323 distribution function, which leads to the SCS curve number method, is used for describing the  
324 spatial distribution of soil water storage capacity. The mean (i.e., average soil water storage  
325 capacity) and the shape parameter (i.e., the spatial variability of soil storage capacity over the  
326 watershed) of the distribution function can be estimated from the available data. Based on the  
327 linkage of the distribution function and the SCS curve number method, a new method based on  
328 the existing observed data of watershed characteristics is proposed for estimating the average soil  
329 water storage capacity. The average soil water storage capacity ( $S_b$ ), as one of the parameters in  
330 the model, was estimated as a function of climate aridity index and curve number which is  
331 calculated based on land cover and soil data.

332 The developed mean annual water balance was applied to diagnose the estimation of shape  
333 parameter ( $a$ ) in this study. The shape parameter, describing the spatial variation of soil water  
334 storage capacity, was first estimated based on the porosity and soil thickness data in the soil  
335 database (gSSURGO). The estimated values of  $a$  were tested in 35 watersheds. The results  
336 showed that the model with the estimated values of  $S_b$  and  $a$  underestimated the mean annual  
337 runoff by 11.8% on average over all the study watersheds. The underestimation of runoff is mainly



338 caused by the underestimation of the spatial heterogeneity of soil thickness over the watershed.  
339 The Height Above the Nearest Drainage (HAND) was then calculated as the total soil thickness  
340 for estimating the total volume of the pore space. The result showed that topography is of great  
341 importance for determining the spatial variability of soil water storage capacity. The estimated  
342 shape parameter from porosity-HAND overestimated the spatial variability of the storage capacity  
343 compared with the calibrated  $a$ , which may result from the assumed bedrock in the HAND method.  
344 Future research will investigate alternative methods for better estimating the spatial variability of  
345 soil water storage capacity over watersheds and test them in the proposed mean annual water  
346 balance model.

347

#### 348 **Data availability**

349 The soil and land use data used in this paper are provided in the references. Daily precipitation,  
350 streamflow, and temperature data are downloaded from  
351 [ftp://hydrology.nws.noaa.gov/pub/gcip/mopex/US\\_Data/](ftp://hydrology.nws.noaa.gov/pub/gcip/mopex/US_Data/).

352

#### 353 **Author contributions**

354 DW designed the analyses. YG and LY conducted the analyses. YG and DW wrote the paper.  
355 LY and NC edited the paper.

356

#### 357 **Competing interests**

358 The authors declare that they have no conflict of interest.

359

#### 360 **Acknowledgements**





361 This research was funded in part by National Science Foundation (award CBET-1804770) and  
362 Florida Department of Transportation.

363 **Reference**

364 Abatzoglou, J. T., and Ficklin, D. L.: Climatic and physiographic controls of spatial variability in  
365 surface water balance over the contiguous United States using the Budyko relationship,  
366 *Water Resour. Res.*, 53(9), 7630-7643, <https://doi.org/10.1002/2017WR020843>, 2017.

367 Alipour, M. H. and Kibler, K. M.: A framework for streamflow prediction in the world's most  
368 severely data-limited regions: test of applicability and performance in a poorly-gauged  
369 region of China, *J. Hydrol.*, 557, 41-54, <https://doi.org/10.1016/j.jhydrol.2017.12.019>,  
370 2018.

371 Alipour, M. H. and Kibler, K. M.: Streamflow prediction under extreme data scarcity: a step  
372 toward hydrologic process understanding within severely data-limited regions, *Hydrolog.  
373 Sci. J.*, 64(9), 1038-1055, <https://doi.org/10.1080/02626667.2019.1626991>, 2019.

374 Atkinson, S. E., Woods, R. A., and Sivapalan, M.: Climate and landscape controls on water balance  
375 model complexity over changing timescales, *Water Resour. Res.*, 38(12),  
376 1314, <https://doi.org/10.1029/2002WR001487>, 2002.

377 Bartlett, M. S., Parolari, A. J., McDonnell, J. J., and Porporato, A.: Beyond the SCS-CN method:  
378 A theoretical framework for spatially lumped rainfall-runoff response, *Water Resour. Res.*,  
379 52(6), 4608-4627, <https://doi.org/10.1002/2015WR018439>, 2016.

380 Berghuijs, W. R., Hartmann, A., and Woods, R. A.: Streamflow sensitivity to water storage  
381 changes across Europe, *Geophys. Res. Lett.*, 43, 1980-1987,  
382 <https://doi.org/10.1002/2016GL067927>, 2016.



- 383 Berghuijs, W. R., Sivapalan, M., Woods, R. A., and Savenije, H. H.: Patterns of similarity of  
384 seasonal water balances: A window into streamflow variability over a range of time scales,  
385 *Water Resour. Res.*, 50(7), 5638-5661, <https://doi.org/10.1002/2014WR015692>, 2014.
- 386 Blöschl, P. G., Sivapalan, P. M., Wagener, P. T., Viglione, D. A., and Savenije, H. H.: *Runoff*  
387 *Prediction in Ungauged Basins: Synthesis across Processes, Places and Scales*, Cambridge  
388 Univ. Press, Cambridge, U. K., 2013.
- 389 Budyko, M.I.: *The Heat Balance of the Earth's Surface*, U.S. Dep. of Commer., Washington, D.  
390 C., 1958.
- 391 Chen, X., Alimohammadi, N., and Wang, D.: Modeling interannual variability of seasonal  
392 evaporation and storage change based on the extended Budyko framework, *Water Resour.*  
393 *Res.*, 49(9), 6067-6078, <https://doi.org/10.1002/wrcr.20493>, 2013.
- 394 Chen, X. and Wang, D.: Modeling seasonal surface runoff and base flow based on the generalized  
395 proportionality hypothesis, *J. Hydrol.*, 527, 367-379,  
396 <https://doi.org/10.1016/j.jhydrol.2015.04.059>, 2015.
- 397 Donohue, R. J., Roderick, M. L., and McVicar, T. R.: On the importance of including vegetation  
398 dynamics in Budyko's hydrological model, *Hydrol. Earth Syst. Sci.*, 11, 983-995,  
399 <https://doi.org/10.5194/hess-11-983-2007>, 2007.
- 400 Duan, Q., Sorooshian, S., and Gupta, V.: Effective and efficient global optimization for conceptual  
401 rainfall-runoff models, *Water Resour. Res.*, 28(4), 1015-1031,  
402 <https://doi.org/10.1029/91WR02985>, 1992.
- 403 Duan, Q., Schaake, J., Andreassian, V., Franks, S., Goteti, G., Gupta, H. V., Gusev, Y. M., Habets,  
404 F., Hall, A., Hay, L., Hogue, T., Huang, M., Leavesley, G., Liang, X., Nasonova, O. N.,  
405 Noilhan, J., Oudin, L., Sorooshian, S., Wagener, T., and Wood, E. F.: Model parameter



- 406 estimation experiment (MOPEX): an overview of science strategy and major results from  
407 the second and third workshops, *J. Hydrol.*, 320, 3-17,  
408 <https://doi.org/10.1016/j.jhydrol.2005.07.031>, 2006.
- 409 Farmer, D., Sivapalan, M., and Jothityangkoon, C.: Climate, soil, and vegetation controls upon the  
410 variability of water balance in temperate and semiarid landscapes: Downward approach to  
411 water balance analysis, *Water Resour. Res.*, 39(2), 1035,  
412 <https://doi.org/10.1029/2001WR000328>, 2003.
- 413 Fu, B. P.: On the calculation of the evaporation from land surface [in Chinese]. *Sci. Atmos. Sin.*  
414 5, 23–31, 1981.
- 415 Fu, J. and Wang, W.: On the lower bound of Budyko curve: The influence of precipitation  
416 seasonality, *J. Hydrol.*, 570, 292–303, <https://doi.org/10.1016/j.jhydrol.2018.12.062>, 2019.
- 417 Gao, H., Hrachowitz, M., Schymanski, S. J., Fenicia, F., Sriwongsitanon, N., and Savenije, H. H.  
418 G.: Climate controls how ecosystems size the root zone storage capacity at catchment scale,  
419 *Geophys. Res. Lett.*, 41, 7916-7923, <https://doi.org/10.1002/2014GL061668>, 2014.
- 420 Gao, H., Hrachowitz, M., Sriwongsitanon, N., Fenicia, F., Gharari, S., and Savenije, H. H.:  
421 Accounting for the influence of vegetation and landscape improves model transferability  
422 in a tropical savannah region, *Water Resour. Res.*, 52(10), 7999-8022,  
423 <https://doi.org/10.1002/2016WR019574>, 2016.
- 424 Gao, H., Birkel, C., Hrachowitz, M., Tetzlaff, D., Soulsby, C., and Savenije, H. H.: A simple  
425 topography-driven and calibration-free runoff generation module, *Hydrol. Earth Syst. Sci.*,  
426 23, 787-809, <https://doi.org/10.5194/hess-23-787-2019>, 2019.



- 427 Gentine, P., D'Odorico, P., Lintner, B. R., Sivandran, G., and Salvucci, G.: Interdependence of  
428 climate, soil, and vegetation as constrained by the Budyko curve, *Geophys. Res. Lett.*, 39,  
429 L19404, <https://doi.org/10.1029/2012GL053492>, 2012.
- 430 Gerrits, A. M. J., Savenije, H. H. G., Veling, E. J. M., and Pfister, L.: Analytical derivation of the  
431 Budyko curve based on rainfall characteristics and a simple evaporation model, *Water*  
432 *Resour. Res.*, 45, W04403, <https://doi.org/10.1029/2008WR007308>, 2009.
- 433 Hargreaves, G. H. and Samani, Z. A.: Reference crop evapotranspiration from temperature, *Appl.*  
434 *Eng. Agric.*, 1(2), 96-99, doi: 10.13031/2013.26773, 1985.
- 435 Hickel, K. and Zhang, L.: Estimating the impact of rainfall seasonality on mean annual water  
436 balance using a top-down approach, *J. Hydrol.*, 331(3-4), 409-424,  
437 <https://doi.org/10.1016/j.jhydrol.2006.05.028>, 2006.
- 438 Homer, C. G., Dewitz, J. A., Yang, L., Jin, S., Danielson, P., Xian, G., Coulston, J., Herold, N. D.,  
439 Wickham, J. D., and Megown, K.: Completion of the 2011 National Land Cover Database  
440 for the conterminous United States-Representing a decade of land cover change  
441 information, *Photogramm. Eng. Rem. S.*, 81(5), 345-354, 2015.
- 442 Huang, M., Liang, X., and Liang, Y.: A transferability study of model parameters for the variable  
443 infiltration capacity land surface scheme, *J. Geophys. Res.*, 108(D22), 8864,  
444 <https://doi.org/10.1029/2003JD003676>, 2003.
- 445 Jothityangkoon, C., Sivapalan, M., and Farmer, D. L.: Process controls of water balance variability  
446 in a large semi-arid catchment: downward approach to hydrological model development,  
447 *J. Hydrol.*, 254(1-4), 174-198, [https://doi.org/10.1016/S0022-1694\(01\)00496-6](https://doi.org/10.1016/S0022-1694(01)00496-6), 2001.



- 448 Li, H. Y., Sivapalan, M., Tian, F., and Harman, C.: Functional approach to exploring climatic and  
449 landscape controls of runoff generation: 1. Behavioral constraints on runoff volume, *Water*  
450 *Resour. Res.*, 50, 9300-9322, <https://doi.org/10.1002/2014WR016307>, 2014.
- 451 Li, D., Pan, M., Cong, Z., Zhang, L., and Wood, E. Vegetation control on water and energy balance  
452 within the Budyko framework, *Water Resour. Res.*, 49, 969-976,  
453 <https://doi.org/10.1002/wrcr.20107>, 2013.
- 454 Li, D.: Assessing the impact of interannual variability of precipitation and potential evaporation  
455 on evapotranspiration, *Adv. Water Resour.*, 70, 1-11,  
456 <https://doi.org/10.1016/j.advwatres.2014.04.012>, 2014.
- 457 Maidment, D. R. (Ed.): *ArcHydro: GIS for Water Resources*, ESRI Press, Redlands, Calif., 2002.
- 458 Milly, P. C. D.: Climate, soil water storage, and the average annual water balance, *Water Resour.*  
459 *Res.*, 30(7), 2143-2156, <https://doi.org/10.1029/94WR00586>, 1994.
- 460 Moore, R. J.: The probability-distributed principle and runoff production at point and basin scales,  
461 *Hydrolog. Sci. J.*, 30(2), 273-297, <https://doi.org/10.1080/02626668509490989>, 1985.
- 462 Pike, J. G.: The estimation of annual runoff from meteorological data in a tropical climate, *J.*  
463 *Hydrol.*, 12, 2116-2123, [https://doi.org/10.1016/0022-1694\(64\)90022-8](https://doi.org/10.1016/0022-1694(64)90022-8), 1964.
- 464 Porporato, A., Daly, E., and Rodriguez-Iturbe, I.: Soil water balance and ecosystem response to  
465 climate change, *Am. Nat.*, 164(5), 625-632, <https://doi.org/10.1086/424970>, 2004.
- 466 Sankarasubramanian, A., and Vogel, R. M.: Annual hydroclimatology of the United States, *Water*  
467 *Resour. Res.*, 38(6), 1083, <https://doi.org/10.1029/2001WR000619>, 2002.
- 468 SCS.: *Hydrology, National Engineering Handbook, Supplement A, Section 4, Chapter 10. Soil*  
469 *Conservation Service, US Department of Agriculture, Washington, DC., 1972.*



- 470 Shao, Q., Traylen, A., and Zhang, L.: Nonparametric method for estimating the effects of climatic  
471 and catchment characteristics on mean annual evapotranspiration, *Water Resour. Res.*, 48,  
472 W03517, <https://doi.org/10.1029/2010WR009610>, 2012.
- 473 Tang, Y. and Wang, D.: Evaluating the role of watershed properties in long-term water balance  
474 through a Budyko equation based on two-stage partitioning of precipitation, *Water Resour.*  
475 *Res.*, 53, 4142–4157, <https://doi.org/10.1002/2016WR019920>, 2017.
- 476 Troch, P., Loon, E. V., and Hilberts, A.: Analytical solutions to a hillslope-storage kinematic wave  
477 equation for subsurface flow, *Adv. Water Resour.*, 25(6), 637-649,  
478 [https://doi.org/10.1016/S0309-1708\(02\)00017-9](https://doi.org/10.1016/S0309-1708(02)00017-9), 2002.
- 479 Troch, P. A., Carrillo, G., Sivapalan, M., Wagner, T., and Sawicz, K.: Climate-vegetation-soil  
480 interactions and long-term hydrologic partitioning: Signatures of catchment co-evolution,  
481 *Hydrol. Earth Syst. Sci.*, 17, 2209-2217, <https://doi.org/10.5194/hess-17-2209-2013>, 2013.
- 482 Turc, L.: Le bilan d'eau des sols: Relation entre les precipitations, l'évaporation et l'écoulement,  
483 *Ann. Agron., Serie A 5*, 491–595, 1954.
- 484 USDA: Gridded Soil Survey Geographic (gSSURGO) Database User Guide, U. S. Dep. of Agric.,  
485 Nat. Resour. Conserv. Serv., Washington, D. C., 2014.
- 486 Wang, D. and Hejazi, M.: Quantifying the relative contribution of the climate and direct human  
487 impacts on mean annual streamflow in the contiguous United States, *Water Resour. Res.*,  
488 47, W00J12, <https://doi.org/10.1029/2010WR010283>, 2011.
- 489 Wang, D. and Tang, Y.: A one-parameter Budyko model for water balance captures emergent  
490 behavior in Darwinian hydrologic models, *Geophys. Res. Lett.*, 41, 4569–4577,  
491 <https://doi.org/10.1002/2014GL060509>, 2014.



- 492 Wang, D.: A new probability density function for spatial distribution of soil water storage capacity  
493 leads to SCS curve number method, *Hydrol. Earth Syst. Sci.*, 22, 6567-6578,  
494 <https://doi.org/10.5194/hess-22-6567-2018>, 2018.
- 495 Wood, E. F., Lettenmaier, D. P., and Zartarian, V. G.: A land-surface hydrology parameterization  
496 with subgrid variability for general circulation models, *J. Geophys. Res.*, 97(D3), 2717-  
497 2728, <https://doi.org/10.1029/91JD01786>, 1992.
- 498 Woods, R.: The relative roles of climate, soil, vegetation and topography in determining seasonal  
499 and long-term catchment dynamics, *Adv. Water Resour. Res.*, 37, 701-708,  
500 [https://doi.org/10.1016/S0309-1708\(02\)00164-1](https://doi.org/10.1016/S0309-1708(02)00164-1), 2003.
- 501 Xing, W., Wang, W., Shao, Q., and Yong, B.: Identification of dominant interactions between  
502 climatic seasonality, catchment characteristics and agricultural activities on Budyko-type  
503 equation parameter estimation, *J. Hydrol.*, 556, 585-599,  
504 <https://doi.org/10.1016/j.jhydrol.2017.11.048>, 2018.
- 505 Yang, H., Yang, D., Lei, Z., and Sun, F.: New analytical derivation of the mean annual water-  
506 energy balance equation, *Water Resour. Res.*, 44, W03410,  
507 <https://doi.org/10.1029/2007WR006135>, 2008.
- 508 Yao, L., Libera, D., Kheimi, M., Sankarasubramanian, A., and Wang, D.: The roles of climate  
509 forcing and its variability on streamflow at daily, monthly, annual, and long-term scales,  
510 *Water Resour. Res.*, <https://doi.org/10.1029/2020WR027111>, 2020.
- 511 Yokoo, Y., Sivapalan, M., and Oki, T.: Investigating the roles of climate seasonality and landscape  
512 characteristics on mean annual and monthly water balances, *J. Hydrol.*, 357(3-4), 255-269,  
513 <https://doi.org/10.1016/j.jhydrol.2008.05.010>, 2008.



514 Zhang, L., Dawes, W. R., and Walker, G. R.: Response of mean annual evapotranspiration to  
515 vegetation changes at catchment scale, *Water Resour. Res.*, 37, 701–708,  
516 <https://doi.org/10.1029/2000WR900325>, 2001.

517 Zhao, R. J.: The Xinanjiang model applied in China, *J. Hydrol.*, 135(1–4), 371–381,  
518 [https://doi.org/10.1016/0022-1694\(92\)90096-E](https://doi.org/10.1016/0022-1694(92)90096-E), 1992.

519

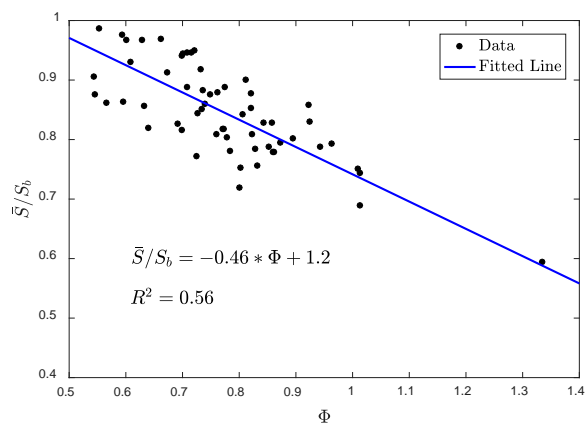




520 Table 1: The USGS gage stations, climate aridity index, the estimated potential maximum  
 521 retention of curve number method ( $S_{CN}$ ), and the average soil water storage capacity ( $S_b$ ) for the  
 522 study watersheds.

Index	Station Name	State	USGS Gauge Number	Climate Aridity Index	$S_{CN}$ (mm)	$S_b$ (mm)
1	Susquehanna River	NY	01503000	0.69	100	862
2	Chemung River	NY	01531000	0.84	95	518
3	Juniata River	PA	01567000	0.85	134	714
4	Rappahannock River	VA	01668000	0.85	152	792
5	Yadkin River	NC	02116500	0.71	153	1221
6	Chattahoochee River	GA	02339500	0.69	182	1559
7	Escambia River	FL	02375500	0.73	143	1075
8	Allegheny River	NY	03011020	0.68	153	1369
9	New River	VA	03168000	0.69	177	1494
10	Great Miami River	OH	03274000	0.89	63	301
11	Eel River	IN	03328500	0.92	68	304
12	East Fork White River	IN	03364000	0.83	68	378
13	Little Wabash River	IL	03381500	0.96	68	279
14	Fox River	WI	04073500	1.12	162	520
15	Auglaize River	OH	04191500	0.98	56	225
16	Maquoketa River	IA	05418500	1.19	72	209
17	Wapsipinicon River	IA	05422000	1.16	69	210
18	Rock River	WI	05430500	1.11	98	316
19	Pecatonica River	IL	05435500	1.11	66	214
20	Kishwaukee River	IL	05440000	1.03	70	255
21	Green River	IL	05447500	1.10	75	247
22	Iowa River	IA	05454500	1.18	65	191
23	Cedar River	IA	05458500	1.17	65	193
24	Kankakee River	IL	05520500	0.93	101	448
25	Fox River	IL	05552500	1.04	88	321
26	Spoon River	IL	05570000	1.12	71	227
27	Kaskaskia River	IL	05592500	0.99	67	263
28	Blue River	KS	06884400	1.70	74	127
29	Thompson River	MO	06899500	1.16	65	195
30	Meramec River	MO	07019000	0.95	109	460
31	Chikaskia River	OK	07152000	1.82	77	121
32	Neosho River	KS	07183000	1.42	63	140
33	Deep Fork River	OK	07243500	1.40	87	197
34	Neches River	TX	08033500	1.14	174	540
35	Elm Fork Trinity River	TX	08055500	1.63	87	159

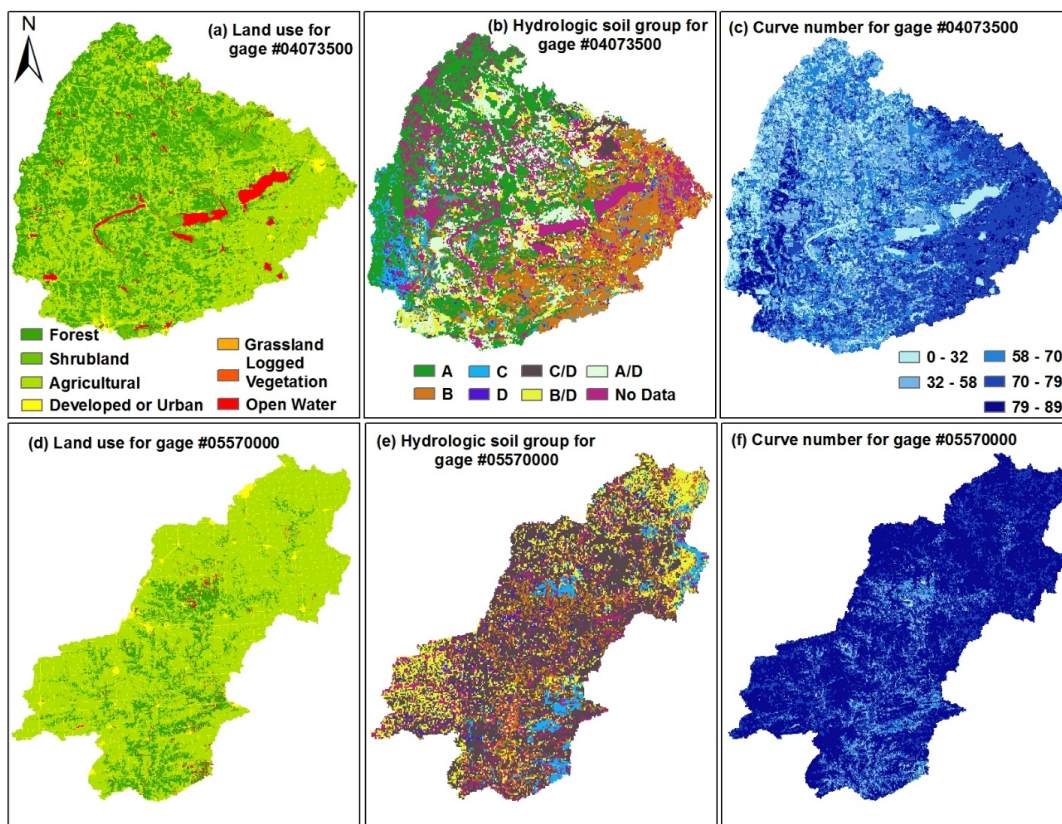
523



524

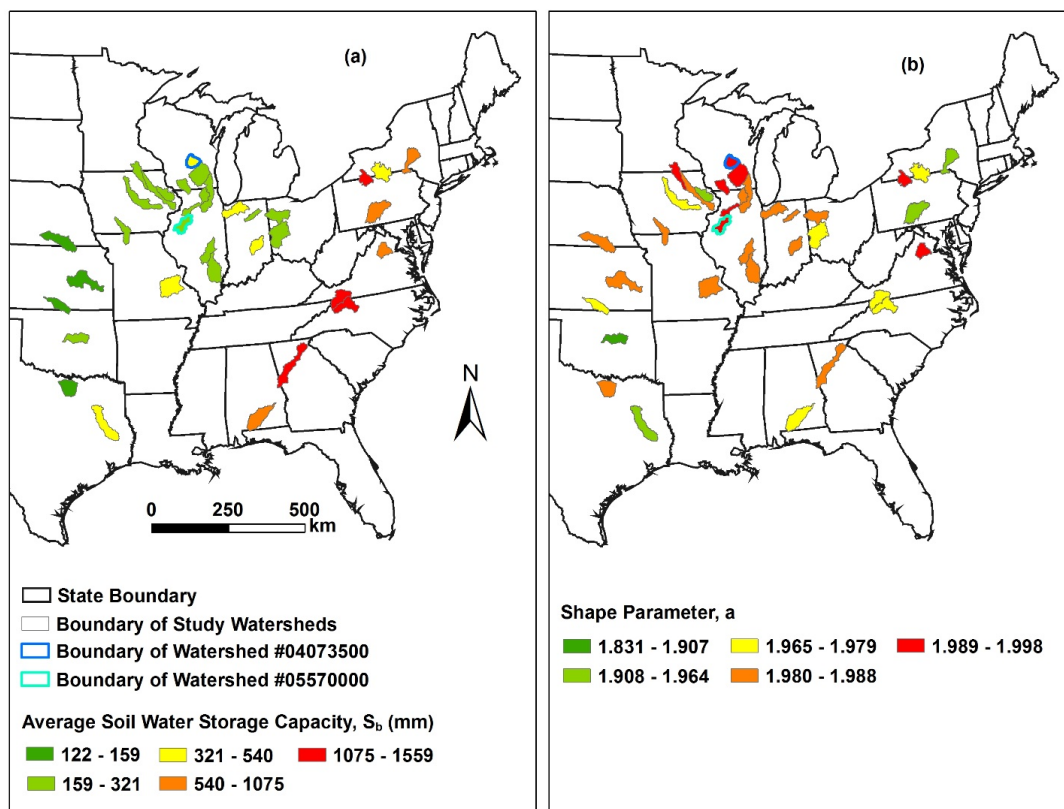
525 Figure 1: The degree of saturation  $\left(\frac{\bar{S}}{S_b}\right)$  under long-term average climate versus climate aridity  
526 index ( $\Phi$ ).

527



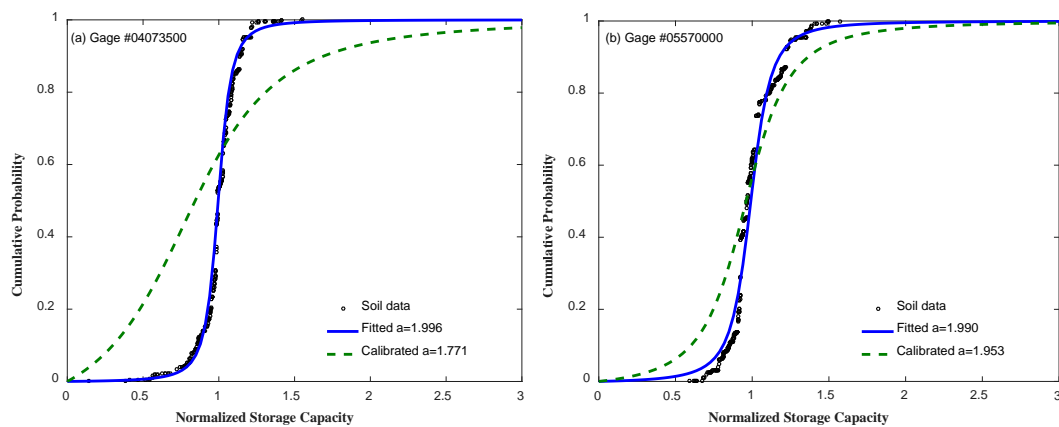
528  
529  
530  
531  
532  
533

Figure 2: The spatial distribution of land use and land cover for Fox River watershed in Wisconsin (a) and Spoon River watershed in Illinois (d), the hydrologic soil groups for Fox River watershed (b) and Spoon River watershed (e), and the curve numbers for Fox River watershed (c) and Spoon River watershed (f).



534  
535  
536  
537

Figure 3: The estimated average soil water storage capacity ( $S_b$ ) as a function of  $S_{CN}$  and climate aridity index (a) and shape parameter from soil data (b).



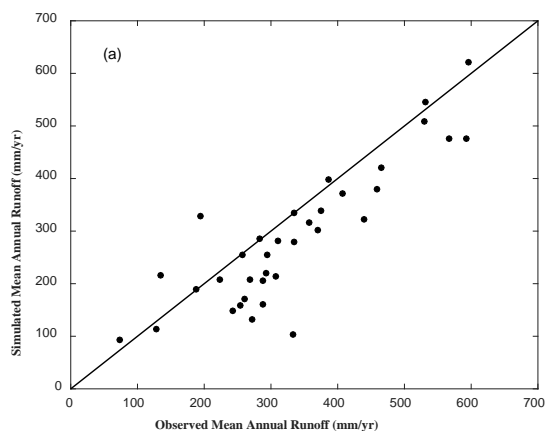
538

539 Figure 4: The estimated shape parameter for the spatial distribution of soil water storage capacity  
540 based on soil data and the calibrated shape parameter based on mean annual water balance in the  
541 Fox River watershed (a) and the Spoon River watershed (b).

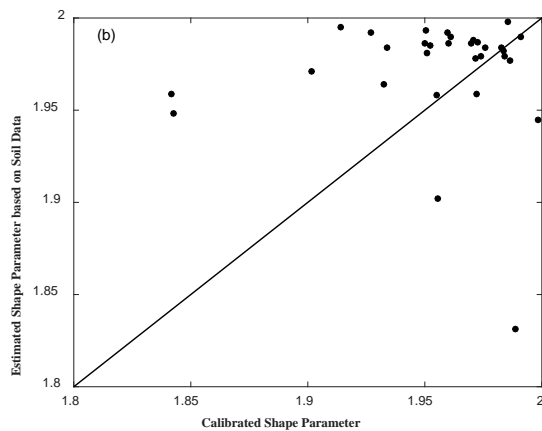
542



543



544



545

546

547

548

549

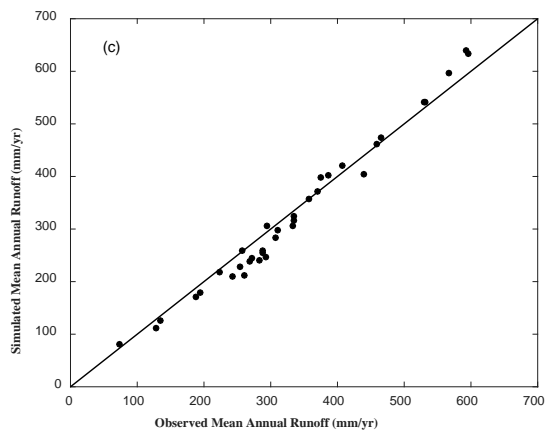
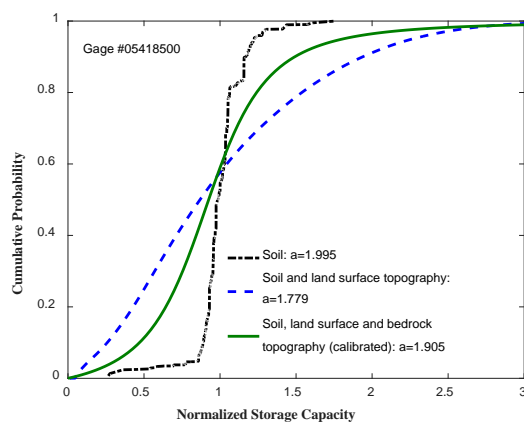


Figure 5: (a) Observed versus simulated mean annual runoff using shape parameter based on soil data; (b) Soil data-based versus calibrated shape parameter; and (c) Observed versus simulated mean annual runoff using shape parameter based on calibration.



550

551 Figure 6: The effects of soil, land surface topography, and bedrock topography on the shape  
552 parameter of the spatial distribution of soil water storage capacity.

553